ISTITUTO NAZIONALE DI RICERCA METROLOGICA
Repository Istituzionale

A correction method for Vickers indenters squareness measurement due to the tilt of the pyramid axis

(Article begins on next page)

19 April 2024

1 **A correction method for Vickers indenters squareness**

2 **measurement due to the tilt of the pyramid axis**

3

4 *Andrea Prato[1], Davide Galliani[2], Claudio Origlia[1] and Alessandro Germak[1]*

5

6 *[1] INRiM - Istituto Nazionale di Ricerca Metrologica, 10135 Torino, Italy*

7 *[2] LTF S.p.A. - 24051 Antegnate (BG), Italy*

8

9 Corresponding author e-mail: *a.prato@inrim.it*

10

11 Abbreviated title: Vickers indenter squareness measurement correction

12

13

14

15

16

17

18

19

20

21

22

23

24

25   **Abstract**

26   In ISO 6507-3 it is required that the quadrilateral base of Vickers indenter has angles of $90° \pm 0.2°$.

27   Squareness angles are usually evaluated through optical techniques by measuring the angles between two

28   consecutive faces, which correspond to the quadrilateral base angles when the axis of the pyramid is perfect-

29   ly parallel to the indenter-holder axis. However, if the pyramid axis is tilted by an angle within 0.3°, as al-

30   lowed by the standard, these angles no longer correspond. This work deals with the description of a numeri-

31   cal method, based on a proper geometrical model, to correct squareness measurements. The proposed method

32   is applied to experimental tests and measurement results, with related uncertainties, are presented. It is

33   shown that the accuracy is improved. This method is easily implementable on different measuring systems

34   and can be internationally adopted to improve the relevant standard.

35

36

37   **Keywords:** Hardness, Vickers indenter, squareness.

38

39

40

41

42

43

44

45

46

47

48

49

50   **1.   Introduction**

51   The influence of indenter characteristics on hardness measurements, in particular for Vickers hardness, is

52   largely reported in literature. It has been demonstrated that different indenters meeting the requirements of

53   the Standards can lead to significantly different hardness measurements, and in particular that an increase in

54   indenter angle entails a decrease in Vickers hardness [1,2]. It was also found that squareness errors and ridge,

55   within the required tolerances, entail small errors in Vickers hardness [3], beyond the influence of the optical

56   system for the evaluation of the indentation impression [4]. Also in Rockwell hardness, it was found that the

57   main causes of differences in performance are due to imperfections in the geometric form of the indenter

58   [5,6], and in particular that an increasing angle of the indenter entails an increase in hardness value [7]. Other

59   works showed that hardness measurements can be affected by the roughness or mechanical deformations of

60   the indenter under load [8] or by form errors of the indenter [9], in Rockwell C, or by friction between the

61   indenter and material for Berkovich and cubic indenters, in microindentation hardness [10].

62   ISO 6507-3 [11] specifies the requirements of the diamond pyramidal indenter used for the calibration of

63   hardness reference blocks. They are composed of a highly polished square-based diamond pyramid with an

64   angle between the opposite faces of the vertex of $136° \pm 0.1°$, placed upon a steel indenter-holder, as shown

65   in Fig. 1.

66

68   **Fig. 1**. 3-D model (left) and picture (right) of a typical Vickers indenter.

69

70   The pyramid quadrilateral base, which is given by the intersection of the faces with a plane perpendicular

71   to the axis of the diamond pyramid, should have angles of $90° \pm 0.2°$. These angles are usually evaluated by

3

72   measuring the angles $\gamma_{\exp,i=1,2,3,4}$ between two consecutive faces, assuming the indenter-holder axis as refer-

73   ence [12,13]. Furthermore, the angle between the pyramid axis and the indenter-holder axis (normal to the

74   seating surface), which represents the tilt angle of the pyramid axis, should be less than 0.3°. Nevertheless,

75   the effect of this tilt on the measurement of the quadrilateral base angles, namely squareness measurement, is

76   not considered in the current international standard. As a matter of fact, when the pyramid axis and indenter-

77   holder axis, normal to the seating surface, are not parallel, the angles $\gamma_{\exp,i}$ between two consecutive faces are

78   different from the quadrilateral base angles $\varphi_{i=1,2,3,4}$. Such behavior affects the accuracy of squareness meas-

79   urement, thus a correction is needed. In this work, a correction method, derived from a proper geometrical

80   model, is proposed and described in the following Sections.

81   **2.   Measurement of Vickers indenters geometry**

82   ISO 6507-3 (Sec. 5.5) requires that the indenter meets some geometrical requirements [11]. These meas-

83   urements are usually performed in calibration laboratories by means of optical measuring systems [12-20]. In

84   particular, the measurement of the four quadrilateral base angles φ_i is performed with microscopes that use

85   angular encoders [21] or with scanning confocal chromatic probes [13]. Both methods use the indenter-

86   holder axis or seating holder as reference. In this condition, measured angles $\gamma_{\exp,i}$ correspond to the actual

87   quadrilateral base angles φ_i when the axis of the pyramid is parallel to the indenter-holder axis, i.e. when it is

88   perpendicular to the seating surface plane. However, these angles are not the same when the pyramid axis is

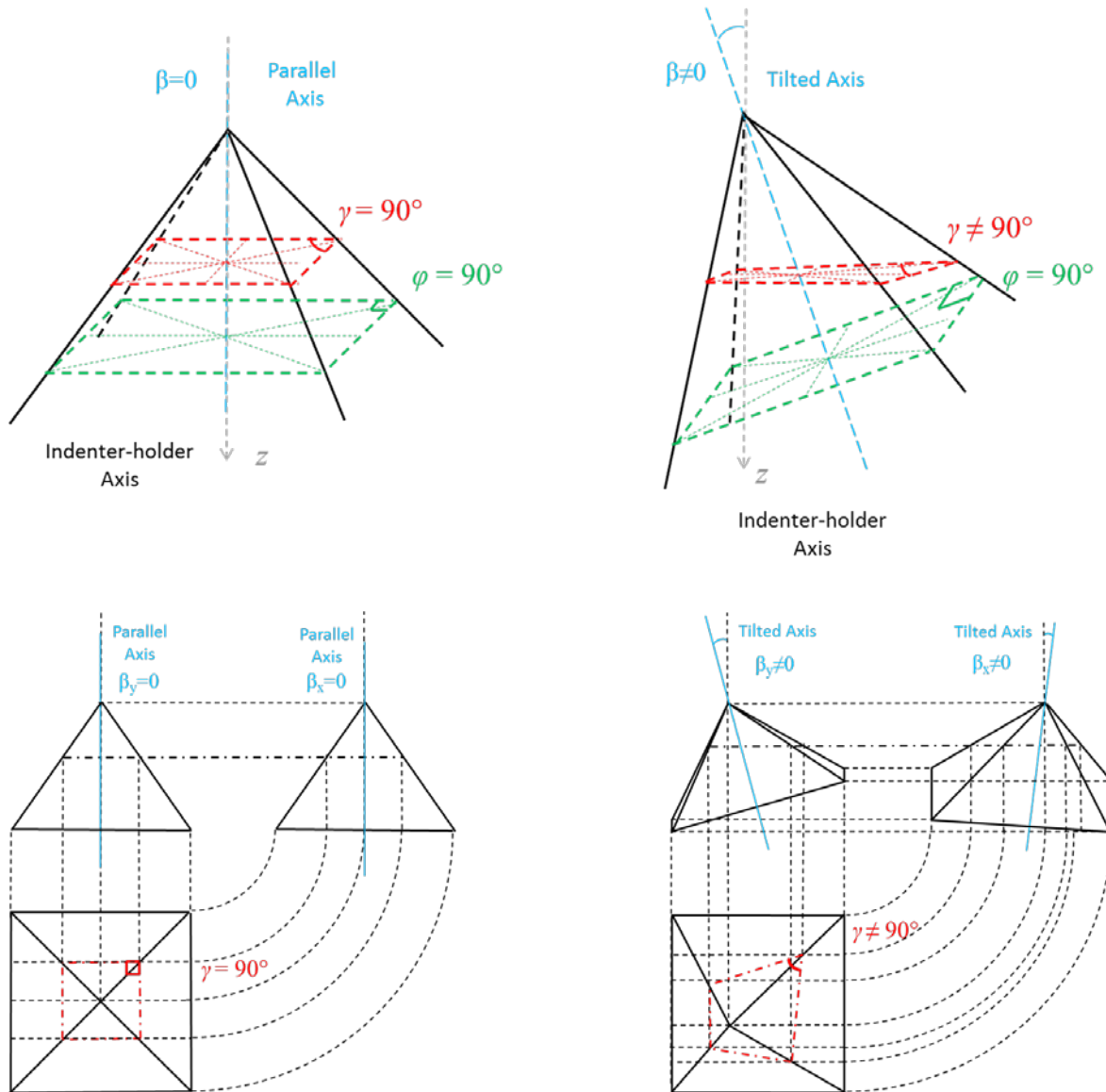89   tilted by an angle β, as shown in Fig. 2.

90

Fig. 2. Representation of a generic pyramid with a parallel axis (left) and a tilted axis (right) with respect to the indenter-holder axis, in cabinet perspective (top) and in orthogonal projection (bottom). The actual square-base angles are depicted in green and the measured angles between two consecutive faces are depicted in red.

By way of example, in INRiM hardness laboratory, the Galileo-LTF® Gal-Indent optical system is adopted (Fig. 3) [12]. This system is able to measure the two vertex angles α_x and α_y of the indenter (nominally 136°) along x- and y- axis, respectively, between two opposite faces, and the four angles $\gamma_{exp,i}$ between two consecutive faces (nominally 90°) by means of two angular encoders mounted on the optical measuring system [21].

102

103

Fig. 3. The Galileo-LTF® Gal-Indent optical system used at INRiM hardness laboratory for the measurement of the vertex angles and the quadrilateral base angles.

106

Its geometrical characteristics assure that all mechanical parts are perfectly aligned and that the Vickers indenter-holder axis is perpendicular to the lens of the system. The optical system is based on Mirau interferometry, where a light beam (wavelength of 546 nm) is split into two beams: one is reflected to the observer (either through the eyepieces or through a TV Camera), the other hits a Vickers indenter lateral face and is reflected to the observer as well. The two beams recombine and generate an interference pattern. The indenter is simultaneously rotated around the axis passing through the pyramid vertex normal to the plane containing the indenter-holder axis and the optical lens axis, and around the indenter-holder axis, until a lateral face is parallel to the plane of the microscope lens by observing the interference fringes. These two rotations are measured by means of two angular encoders. Rotations around the indenter-holder axis represent the meas-

116 urement of the angles $\gamma_{\text{exp},i}$ between two consecutive faces, whereas, for each lateral face, rotations around

117 the axis passing through the pyramid vertex normal to the plane containing the indenter-holder axis and the

118 optical lens axis represent the measurement of the supplementary angles $(\omega_{x-}, \omega_{x+}, \omega_{y-}, \omega_{y+})$ along x- and y-

119 axis in clockwise (-) and counter clockwise (+) directions, according to Fig. 4. In this way, the two vertex

120 angles α_x and α_y and the pyramid tilt angles β_x and β_y, along x- and y- axis, can be calculated, respectively,

121 according to to Eqs. (1) and Eqs. (2). By way of example, in Fig. 4, the cross-section of a Vickers indenter

122 through yz plane shows the measured vertex angle α_y and the tilt angle β_y.

123   By decomposing the pyramid tilted axis vector **v** along xz and yz planes, according to Fig. 5, Eq. (3) and

124 Eq. (4) can be derived and combined. From Eq. (4), it is then possible to derive the relationship between the

125 total tilt angle β and the pyramid tilt angles β_x and β_y, along x- and y- axis, as shown in Eq. (5), which, in

126 turn, can be approximated to Eq. (6) by applying small-angle approximation as the angle between the pyra-

127 mid axis and the indenter-holder axis is in the order of 10^{-1} °.

128

$$\alpha_x = 180 - (\omega_{x+} + \omega_{x-}); \qquad \alpha_y = 180 - (\omega_{y+} + \omega_{y-}) \tag{1}$$

129

$$\beta_x = \frac{\omega_{x+} - \omega_{x-}}{2}; \;\; \beta_y = \frac{\omega_{y+} - \omega_{y-}}{2} \tag{2}$$

130

$$\|\mathbf{v}\| \cos \beta = \|\mathbf{v_{xz}}\| \cos \beta_x = \|\mathbf{v_{yz}}\| \cos \beta_y \tag{3}$$

131

$$\|\mathbf{v}\| \sin \beta = \sqrt{(\|\mathbf{v_{xz}}\| \sin \beta_x)^2 + (\|\mathbf{v_{yz}}\| \sin \beta_y)^2} =$$
$$= \sqrt{\left(\frac{\|\mathbf{v}\| \cos \beta}{\cos \beta_x} \sin \beta_x\right)^2 + \left(\frac{\|\mathbf{v}\| \cos \beta}{\cos \beta_y} \sin \beta_y\right)^2} = \|\mathbf{v}\| \cos \beta \sqrt{\left(\frac{\sin \beta_x}{\cos \beta_x}\right)^2 + \left(\frac{\sin \beta_y}{\cos \beta_y}\right)^2} \tag{4}$$

132

$$\tan \beta = \sqrt{(\tan \beta_x)^2 + (\tan \beta_y)^2} \tag{5}$$

133

$$\beta = \sqrt{\beta_x{}^2 + \beta_y{}^2} \tag{6}$$
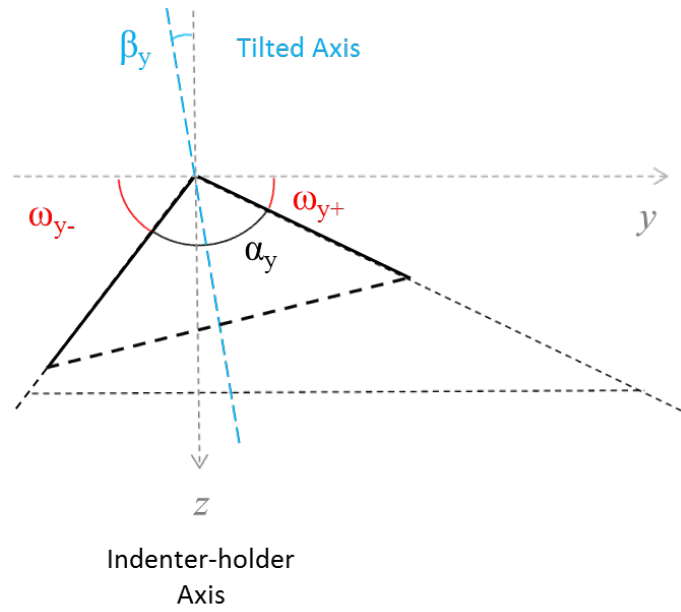
134

135

136   **Fig. 4.** Cross-section of Vickers indenter angles measured with the optical system through *yz* plane.
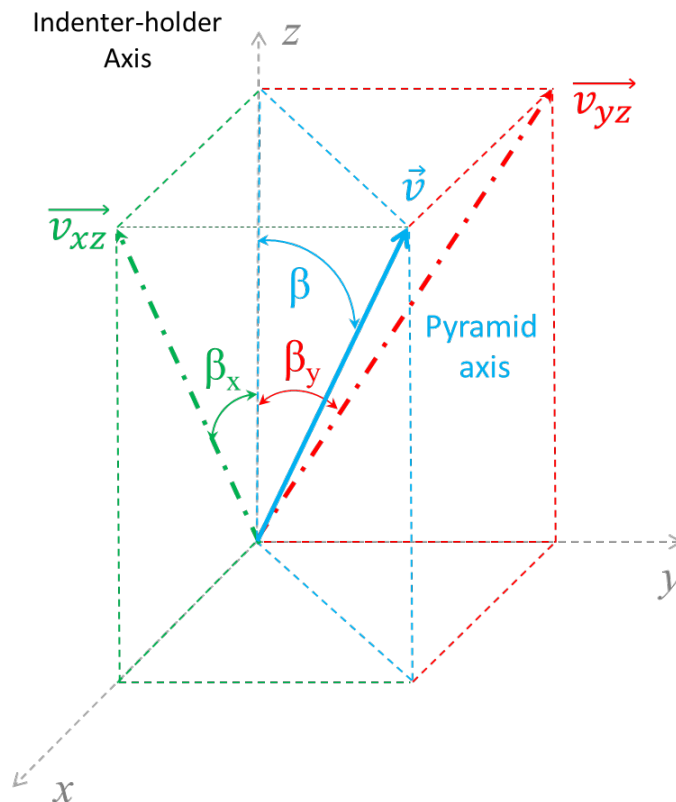
137

138

139   **Fig. 5.** Decomposition of the tilted pyramid axis vector **v** and the associated angles along *x*- and *y*- axis.

140

3.   Correction method

The geometrical model at the base of the correction method aims to calculate the theoretical angles γ_i of an ideal square-based pyramid with a tilted axis with respect to the indenter-holder axis, and correct the measured quadrilateral base angles $\gamma_{\exp,i}$. The following equations are based on fundamental elements of linear algebra [22].

Firstly, by cutting the tilted pyramid with a horizontal plane (z = 1) perpendicular to the indenter-holder axis unit vector **k** = (0,0,1), the vectors **v'** and $\mathbf{p}_{i=1,2,3,4}$, which represent the vectors of the bisector between the indenter-holder axis **k** and the pyramid axis **v**, and the four lateral edges of the associated right pyramid, respectively, are defined according to Eqs. (7). Vectors are shown in Fig. 6 (left) and Fig. 7 (top-left). The bisector between the indenter-holder axis **k** and the pyramid axis **v** is used to perform the rotation of the lateral edge vectors $\mathbf{p}_i$ by finding its symmetrical vectors $\mathbf{q}_i$, as described below.

$$
\begin{cases}
\mathbf{v'} = \left(v'_x, v'_y, v'_z \right) = \left(\tan\dfrac{\beta_x}{2}, \tan\dfrac{\beta_y}{2}, 1 \right) \\[2mm]
\mathbf{p_1} = \left(p_{1x}, p_{1y}, p_{1z} \right) = \left(\tan\dfrac{\alpha_x}{2}, -\tan\dfrac{\alpha_y}{2}, 1 \right) \\[2mm]
\mathbf{p_2} = \left(p_{2x}, p_{2y}, p_{2z} \right) = \left(\tan\dfrac{\alpha_x}{2}, \tan\dfrac{\alpha_y}{2}, 1 \right) \\[2mm]
\mathbf{p_3} = \left(p_{3x}, p_{3y}, p_{3z} \right) = \left(-\tan\dfrac{\alpha_x}{2}, \tan\dfrac{\alpha_y}{2}, 1 \right) \\[2mm]
\mathbf{p_4} = \left(p_{4x}, p_{4y}, p_{4z} \right) = \left(-\tan\dfrac{\alpha_x}{2}, -\tan\dfrac{\alpha_y}{2}, 1 \right)
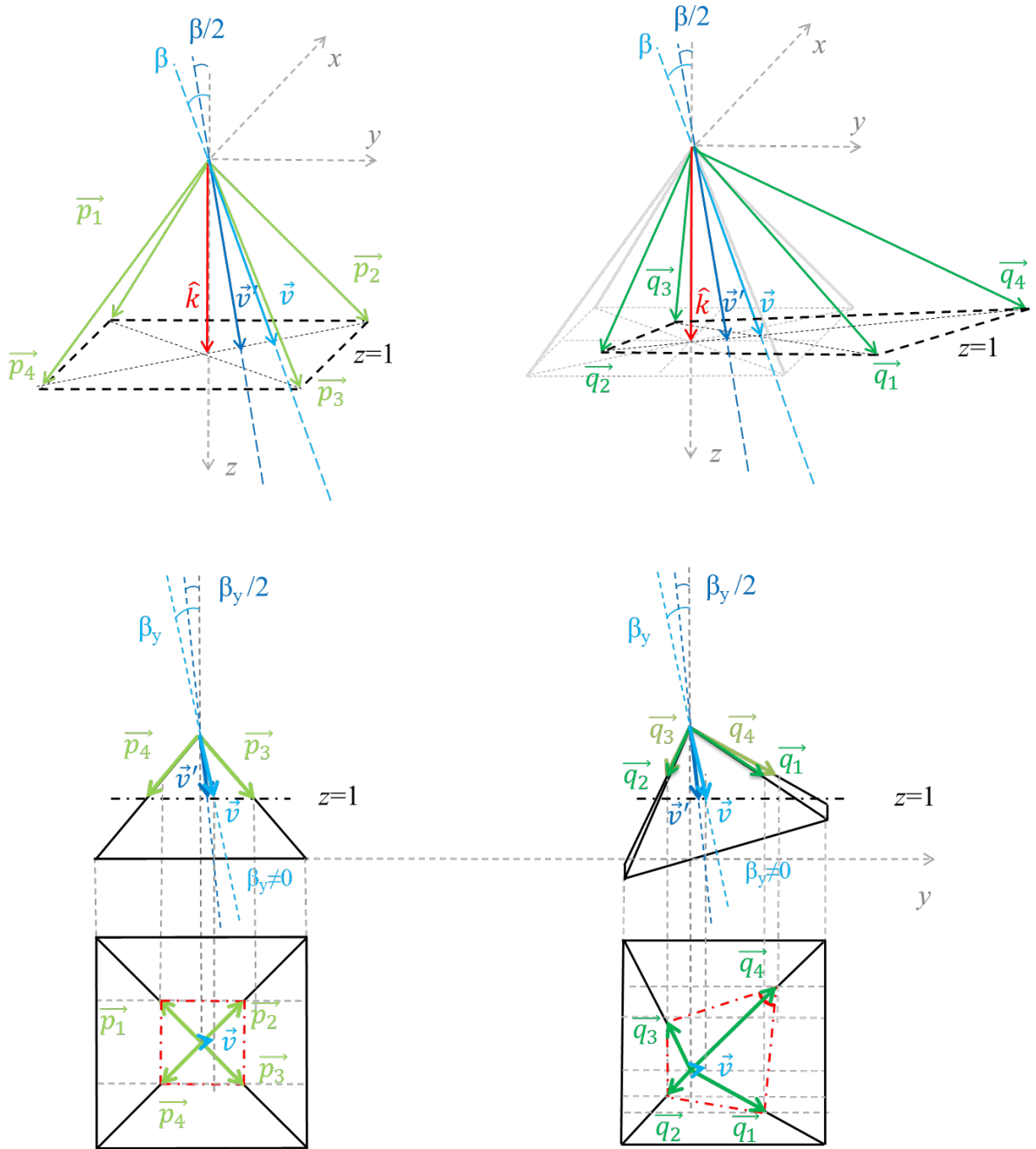\end{cases}
\tag{7}
$$

Fig. 6. Vectors of the associated right pyramid (left) and the tilted pyramid (right) in cabinet perspective (top) and in orthogonal projection (bottom).

By tilting the pyramid by an angle β, the vectors $\mathbf{p_{v',i}}$, which represent the projection of $\mathbf{p_i}$ on $\mathbf{v'}$, can be defined according to Eq. (8) and are shown in Fig. 7 (top-right).

$$\mathbf{p_{v',i}} = \left(p_{v',ix}, p_{v',iy}, p_{v',iz} \right) =$$

(8)

$$= \left(\left(\mathbf{p_i} \cdot \frac{\mathbf{v'}}{\|\mathbf{v'}\|} \right) \frac{\mathrm{v'_x}}{\|\mathbf{v'}\|} , \left(\mathbf{p_i} \cdot \frac{\mathbf{v'}}{\|\mathbf{v'}\|} \right) \frac{\mathrm{v'_y}}{\|\mathbf{v'}\|} , \left(\mathbf{p_i} \cdot \frac{\mathbf{v'}}{\|\mathbf{v'}\|} \right) \frac{\mathrm{v'_z}}{\|\mathbf{v'}\|} \right)$$

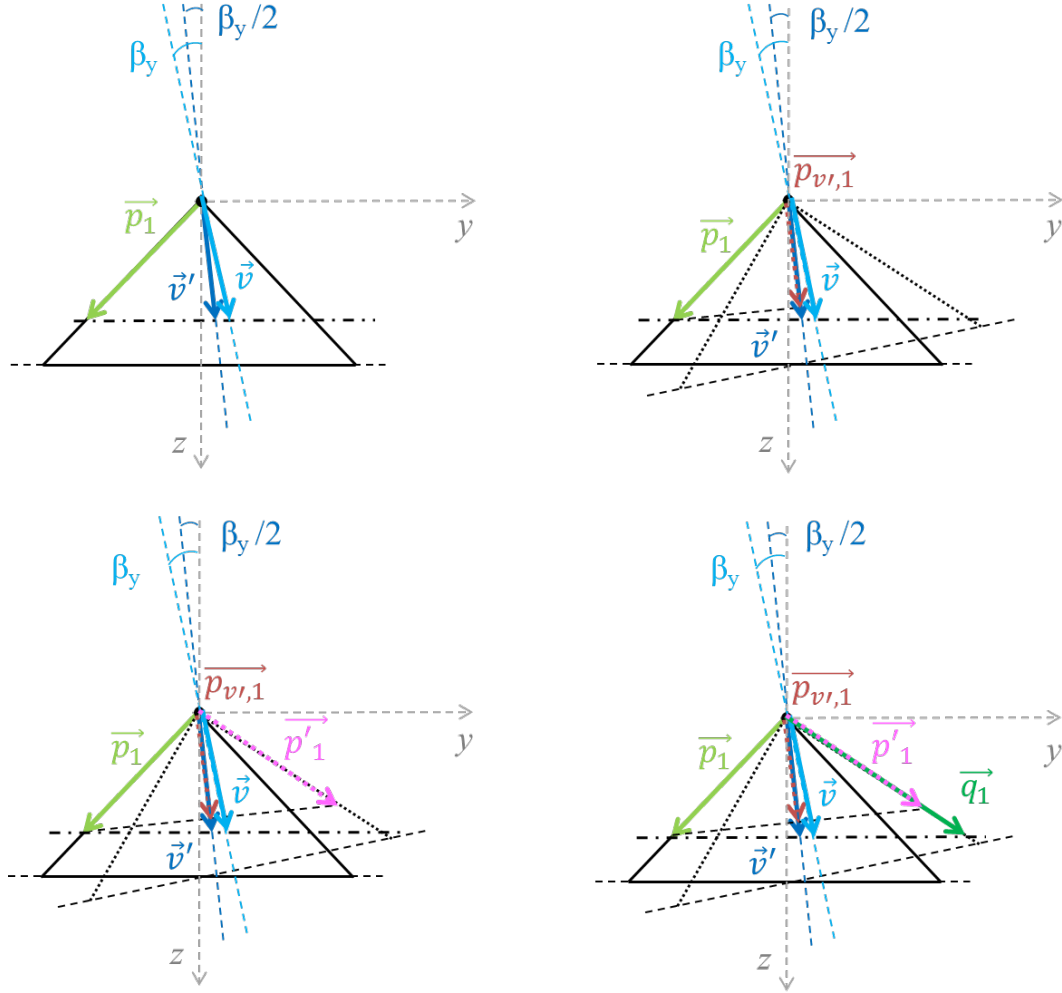161

162

163   **Fig. 7.** Defined vectors (for *i*=1) on the *yz* plane cross-section.

164

165   Considering the tip of vector $\mathbf{p_{v',i}}$ as the midpoint, it is possible to get the lateral edge vectors $\mathbf{p'_i}$ symmet-

166   rical to $\mathbf{p_i}$, according to Eq. (9), as depicted in Fig. 7 (bottom-left).

167

$$\mathbf{p'_i} = \left(\mathrm{p'_{ix}}, \mathrm{p'_{iy}}, \mathrm{p'_{iz}} \right) = \left(2\mathrm{p_{v',ix}} - \mathrm{p_{ix}} , 2\mathrm{p_{v',iy}} - \mathrm{p_{iy}} , 2\mathrm{p_{v',iz}} - \mathrm{p_{iz}} \right) =$$

$$= \left(2 \left(\mathbf{p_i} \cdot \frac{\mathbf{v'}}{\|\mathbf{v'}\|} \right) \frac{\mathrm{v'_x}}{\|\mathbf{v'}\|} - \mathrm{p_{ix}} , 2 \left(\mathbf{p_i} \cdot \frac{\mathbf{v'}}{\|\mathbf{v'}\|} \right) \frac{\mathrm{v'_y}}{\|\mathbf{v'}\|} - \mathrm{p_{iy}} , 2 \left(\mathbf{p_i} \cdot \frac{\mathbf{v'}}{\|\mathbf{v'}\|} \right) \frac{\mathrm{v'_z}}{\|\mathbf{v'}\|} - \mathrm{p_{iz}} \right)$$

(9)

168   Then, by stretching the vectors **p'**$_i$ to the plane $z=1$ and reminding that $p_{iz}=1$, it is possible to obtain the

169   vectors **q**$_i$, which represent the lateral edge vectors of the tilted square-base pyramid, according to Eq. (10).

170   These vectors are represented in Fig. 6 (right) and Fig.7 (bottom-right).

171

$$\mathbf{q_i} = (q_{ix}, q_{iy}, q_{iz}) = \left(\frac{2\left(\mathbf{p_i} \cdot \frac{\mathbf{v'}}{\|\mathbf{v'}\|}\right)\frac{v_x'}{\|\mathbf{v'}\|} - p_{ix}}{2\left(\mathbf{p_i} \cdot \frac{\mathbf{v'}}{\|\mathbf{v'}\|}\right)\frac{v_z'}{\|\mathbf{v'}\|} - p_{iz}}, \frac{2\left(\mathbf{p_i} \cdot \frac{\mathbf{v'}}{\|\mathbf{v'}\|}\right)\frac{v_y'}{\|\mathbf{v'}\|} - p_{iy}}{2\left(\mathbf{p_i} \cdot \frac{v_z'}{\|\mathbf{v'}\|}\right)\frac{v_z'}{\|\mathbf{v'}\|} - p_{iz}}, 1 \right) =$$

$$= \left(\frac{2(\mathbf{p_i} \cdot \mathbf{v'})v_x' - p_{ix}\|\mathbf{v}\|^2}{2(\mathbf{p_i} \cdot \mathbf{v'})v_z' - p_{iz}\|\mathbf{v}\|^2}, \frac{2(\mathbf{p_i} \cdot \mathbf{v'})v_y' - p_{iy}\|\mathbf{v'}\|^2}{2(\mathbf{p_i} \cdot \mathbf{v'})v_z' - p_{iz}\|\mathbf{v'}\|^2}, 1 \right) = \tag{10}$$

$$= \left(\frac{2(\mathbf{p_i} \cdot \mathbf{v'})v_x' - p_{ix}\|\mathbf{v'}\|^2}{2(\mathbf{p_i} \cdot \mathbf{v'}) - \|\mathbf{v'}\|^2}, \frac{2(\mathbf{p_i} \cdot \mathbf{v'})v_y' - p_{iy}\|\mathbf{v'}\|^2}{2(\mathbf{p_i} \cdot \mathbf{v'}) - \|\mathbf{v'}\|^2}, 1 \right)$$

172

173   By subtracting two consecutive vectors **q**$_i$, the quadrilateral base vectors **r**$_i$ are obtained according to

174   Eqs. (11), and the theoretical angles γ_i of a tilted square-based pyramid can thus be found according to

175   Eqs. (12) (see Fig. 8).

176

$$\begin{cases} \mathbf{r_{i=1,2,3}} = \mathbf{q_i} - \mathbf{q_{i+1}} \\ \mathbf{r_4} = \mathbf{q_4} - \mathbf{q_1} \end{cases} \tag{11}$$

177

$$\begin{cases} \gamma_{i=1,2,3} = \cos^{-1}\left(\frac{\mathbf{r_i} \cdot (-\mathbf{r_{i+1}})}{\|\mathbf{r_i}\| \cdot \|\mathbf{r_{i+1}}\|} \right) \\ \gamma_4 = 360 - \gamma_1 - \gamma_2 - \gamma_3 \end{cases} \tag{12}$$
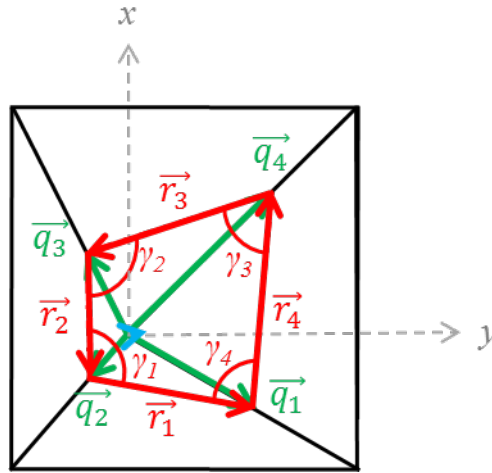
Fig. 8. Quadrilateral base vectors and angles.

In this way, the measured angles $\gamma_{exp,i}$ can be corrected and the actual angles φ_i of the quadrilateral base of the tilted pyramid can be numerically evaluated according to Eq. (13).

$$\varphi_i = 90 + \gamma_{exp,i} - \gamma_i \qquad (13)$$

4.   Measurement results and associated uncertainty

In this Section, the application of the numerical correction method to experimental squareness measurements is presented. The Vickers indenter under test is a Galileo-LTF® indenter. Measurements are performed at INRiM with the Galileo-LTF® Gal-Indent optical system, described in Section 2. Currently, at international level, traceability of Vickers diamond indenter angle measurements, according to ISO 6507-3, are guaranteed by INRiM with absolute expanded uncertainties ($k = 2$, 95 % of confidence level) of 0.05° for the tilt angle β, for the angles between the opposite faces of the vertex α and for the angles of the quadrilateral base $\gamma_{exp,i}$.

In this illustrative case, the measured supplementary angles of the diamond pyramidal indenter along x- and y- directions ($\omega_{x+}, \omega_{x-}, \omega_{y+}, \omega_{y-}$) are 21.980°, 22.089°, 22.131° and 21.955°, respectively, and the measured squareness angles between two consecutive faces ($\gamma_{exp,1}, \gamma_{exp,2}, \gamma_{exp,3}, \gamma_{exp,4}$) are 90.11°, 90.38°, 89.95° and 89.57°, respectively. According to Eq. (1), the measured vertex angles α_x and α_y of the indenter along x-

196 and y-axis are 135.93° and 135.91°, respectively. Both are within the corresponding tolerance interval (136°

197 $\pm$ 0.1°). The tilt angles β_x and β_y, evaluated according to Eq. (2), are -0.05° and 0.09°, respectively, thus the

198 total tilt angle is 0.10°, according to Eq. (6), which is within the standard tolerance of 0.30°. These data are

199 used as inputs in the previous equations and, in this way, the theoretical angles of the associated square-base

200 pyramid γ_i can be found.

201   Squareness angles $\gamma_{exp,i}$, theoretical angles of the associated tilted square-base pyramid γ_i, and the cor-

202 rected angles φ_i, according to Eq. (13), along with the expanded uncertainties (coverage factor, k=2) evaluat-

203 ed according to GUM [23], are listed in Table 1.

204   It is observed that without the correction, two angles (2 and 4) are outside the tolerance interval. The dif-

205 ference between corrected and measured angles (φ_i-$\gamma_{exp,i}$) to show the magnitude of correction, and the dif-

206 ference between corrected angles φ_i and 90° to verify the compliance with the requirement of the relevant

207 standard, are also reported. It is shown that the maximum correction is 0.35° and that the application of the

208 proposed procedure allows, in this illustrative case, to fulfill the standard requirements.

209

210 **Table 1**

211 Experimental squareness measurement with the implementation of the correction method.

Angle i	Measured angle $\gamma_{exp,i}$ / °	Theoretical angle γ_i / °	Corrected angle φ_i / °	φ_i - $\gamma_{exp,i}$ / °	φ_i - 90 / °
1	90.11 $\pm$ 0.05	90.10 $\pm$ 0.03	90.01 $\pm$ 0.06	-0.10 $\pm$ 0.06	0.01 $\pm$ 0.06
2	90.38 $\pm$ 0.05	90.34 $\pm$ 0.03	90.04 $\pm$ 0.06	-0.34 $\pm$ 0.06	0.04 $\pm$ 0.06
3	89.95 $\pm$ 0.05	89.90 $\pm$ 0.03	90.05 $\pm$ 0.06	0.10 $\pm$ 0.06	0.05 $\pm$ 0.06
4	89.57 $\pm$ 0.05	89.65 $\pm$ 0.03	89.92 $\pm$ 0.06	0.35 $\pm$ 0.06	-0.08 $\pm$ 0.06

212

213 **5. Conclusions**

214   ISO 6507-3 specifies that the quadrilateral base of the diamond pyramidal Vickers indenter used for the

215 calibration of hardness reference blocks has angles of 90° ± 0.2°. This measurement is usually performed

216 with optical techniques by measuring the angles between two consecutive lateral faces, using the indenter-

217 holder axis or seating holder as reference. However, if the pyramid axis is tilted by a maximum angle of 0.3°

218 with respect to the indenter-holder axis, as allowed by the standard, squareness measurement is not accurate

219 enough. In fact, in this case, the actual quadrilateral base angles do not correspond to the angles between two

220 consecutive faces. Such behavior affects the accuracy of squareness measurement, thus a correction is need-

221 ed. In this work, a numerical correction method, derived from a proper geometrical model of the Vickers

222 indenter, is finally proposed and described to overcome this issue. Its implementation on experimental meas-

223 urements, reported along with the associated uncertainties, shows that the correction method improves the

224 accuracy of Vickers indenters squareness measurement. Furthermore, since it is suitable for different measur-

225 ing systems and is easily implementable, even on common spreadsheets, the method can be adopted interna-

226 tionally, in the future, to improve the relevant standard. Future works will be aimed at extending the correc-

227 tion method for Rockwell and Berkovich indenters and at evaluating more in-depth the direct influence of

228 squareness and tilt errors on Vickers hardness tests.

232 **References**

233 [1] L. Brice, The influence of indenter characteristics on hardness measurements, in: Proceedings of XVII

234 IMEKO World Congress Metrology, Dubrovnik, Croatia, June 22-27, 2003.

235 [2] M. El-Sherbiny, R. Hegazy, M. Ibrahim, and A. Abuelezz, The influence of geometrical tolerances of

236 Vickers indenter on the accuracy of measured hardness, Int. J. Metrol. Qual. Eng. 3 (2012) 1–6.

237   [3] F. Petik, Factors influencing hardness measurement (a systematic survey of research results), Bureau

238   International de Metrologie Legale, Paris, (1983).

239   [4] G. Barbato, S. Desogus, Problems in the measurement of Vickers and Brinell indentations, Measurement

240   4(4) (1986) 137-147.

241   [5] G. Barbato, F. Petik, Metrological involvement in the definition and dissemination of hardness scales, in:

242   Proceedings of XIII IMEKO, vol. 1, Torino, 1994, pp. 761–766.

243   [6] R.S. Marriner, J.G. Wood, Investigation into the measurement and performance of Rockwell C diamond

244   indenters, Metallurgia 87 (1967) 87–90.

245   [7] G. Barbato, S. Desogus, R. Levi, The meaning of the geometry of Rockwell indenters, IMGC Tech. Rep.

246   R128 (1978).

247   [8] G. Barbato, M. Galetto, A. Germak, F. Mazzoleni, Influence of the indenter shape in Rockwell hardness

248   test, in: Proceedings of the HARDMEKO '98, September 21–23, Beijing, China, 1998, pp. 53–60.

249   [9] J. Song, S. Low, L. Ma, Form error and hardness performance of Rockwell diamond indenters, in: Pro-

250   ceedings of 16th World Congress of International Measurement Confederation (IMEKO XVI), Vienna, Aus-

251   tria, September 01, 2000, p. 6.

252   [10]   J. Qin, Y. Huang, K.C. Hwang, J. Song, G.M. Pharr, The effect of indenter angle on the microindenta-

253   tion hardness, Acta Materialia 55 (2007) 6127–6132.

254   [11] ISO 6507-3:2018 Metallic materials - Vickers hardness test - Part 3: Calibration of reference blocks.

255   [12]   A. Liguori, A. Germak, G. Gori, E. Messina, Galindent: the reference metrological system for the veri-

256   fication of the geometrical characteristics of Rockwell and Vickers diamond indenters, In: VDI/VDE-GMA,

257   IMEKO TC3/TC5/TC20 Joint International Conference, 24-26 Sept. 2002, VDI-Berichte 1685, Tagung Cel-

258   le, Germany, 2002, pp. 365-371.

259   [13]   T. Sanponpute, W. Limthunyalak, F. Menelao, D. Schwenk, Vickers indenter shape measurement by

260   using scanning confocal chromatic instrument, in: Proceedings of XXI IMEKO World Congress "Measure-

261   ment in Research and Industry", Prague, Czech Republic, August 30 - September 4, 2015.

262 [14]   R. Affri, S. Desogus, A. Germak, F. Mazzoleni, D. Perteghella, Optical measuring system for hardness

263 indenters, in: Proceedings of XVI IMEKO World Congress Measurement, Vienna, Austria, September 25-

264 28, 2000.

265 [15]   S. Takagi, K. Kamijo, T. Usuda, H. Kawachi, K. Hanaki, Wide-range verification of the geometry of

266 Vickers diamond indenters, in: Proceedings of XVIII IMEKO World Congress Measurement, Rio de Janeiro,

267 Brazil, September 17-22, 2006.

268 [16]   S. Takagi, T. Ishibashi, Analysis of indenter geometry verification data by means of the regression

269 plane fitting, in: Proceedings of IMEKO 2010 TC3, TC5 and TC22 Conferences Metrology in Modern Con-

270 text, Pattaya, Chonburi, Thailand, November 22−25, 2010.

271 [17]   K. Hasche, K. Herrmann, F. Pohlenz, K. Thiele, Determination of the geometry of microhardness in-

272 denters with a scanning force microscope, Meas. Sci. Technol. 9 (1998) 1082–1086.

273 [18]   A. Germak, K. Herrmann, G. Dai, Z. Li, Development of calibration methods for hardness indenters,

274 VDI-Berichte 1948, 2006, pp. 13–26..

275 [19] L. Zhang, Y. Cui, F. Zhang, Optical measuring system for the geometrical parameters of Rockwell and

276 Vickers diamond hardness indenters, in: Proceedings of LIDAR Imaging Detection and Target Recognition

277 Volume 10605, Changchun, China, 23-25 July, 2017.

278 [20]   A. Germak, C. Origlia, Investigations of new possibilities in the calibration of diamond hardness in-

279 denters geometry, Measurement 44 (2011) 351–358.

280 [21]   A. Germak, A. Liguori, C. Origlia, Experience in the metrological characterization of primary hard-

281 ness standard machines, in: Proceedings of HARDMEKO 2007, Tsukuba, Japan, November 19-21, 2007,

282 pp. 81-89.

283 [22]   S. Lipschutz, M.L. Lipson, Linear Algebra, fifth ed., Mc Graw Hill, New York, 2009.

284 [23]   JCGM 100:2008, Evaluation of Measurement Data — Guide to the Expression of Uncertainty in

285 Measurement (GUM), Joint Committee for Guides in Metrology, Sèvres, France.